Toward a Comprehensive Model of the Synthesis of TiO 2 Particles from TiCl 4

6 AUTHORS, INCLUDING:

Richard Henry West
Northeastern University
30 PUBLICATIONS **394** CITATIONS

Oliver R Inderwildi
University of Oxford
48 PUBLICATIONS **1,083** CITATIONS

Markus Kraft
University of Cambridge
213 PUBLICATIONS **3,035** CITATIONS

Toward a Comprehensive Model of the Synthesis of TiO₂ Particles from TiCl₄

Richard H. West, Matthew S. Celnik, Oliver R. Inderwildi, and Markus Kraft*

Department of Chemical Engineering, University of Cambridge, Cambridge CB2 3RA, United Kingdom

Gregory J. O. Beran and William H. Green

Massachusetts Institute of Technology, 77 Massachusetts Avenue, Cambridge, Massachusetts 02139

The combustion of TiCl₄ to synthesize TiO₂ nanoparticles is a multimillion tonne per year industrial process. The objective of this paper is to further the understanding of this process. Work toward three aspects of this multiscale problem is presented herein: gas-phase chemistry, surface chemistry, and the solution of a multidimensional population balance problem coupled to detailed chemical mechanisms. Presented here is the first thermodynamically consistent mechanism with physically realistic elementary-step rate constants by which TiCl₄ is oxidized to form a stable Ti₂OₓClᵧ species that lies on the path to formation of TiO₂ nanoparticles. Second, progress toward a surface chemistry mechanism based on density functional theory (DFT) calculations is described. Third, the extension of a stochastic two-dimensional (surface−volume) population balance solver is presented. For the first time, the number and size of primary particles within each agglomerate particle in the population is tracked. The particle model, which incorporates inception, coagulation, growth, and sintering, is coupled to the new gas-phase kinetic model using operator splitting, and is used to simulate a heated furnace laboratory reactor and an industrial reactor. Using the primary particle information, transmission electron microscopy (TEM)-style images of the particles are generated, demonstrating the potential utility of first-principles modeling for the prediction of particle morphology in complex industrial systems.

1. Introduction

Titanium dioxide (TiO₂) is widely used as a pigment, a catalyst support, and a photocatalyst. The combustion of titanium tetrachloride (TiCl₄) to synthesize TiO₂ nanoparticles is a multimillion tonne per year industrial process.[1] In this "chloride" process, purified TiCl₄ is oxidized at high temperatures (1500−2000 K) in a pure oxygen plasma or flame to produce TiO₂ particles.[2,3]

The size and shape of these particles affects properties that are important to both the industrial processing and the final product, such as ease of milling[2] and opacity of the powder.[3] Furthermore, the ability to control characteristics of specialized functional nanoparticles through flame synthesis would offer considerable financial reward. As such, the ability to simulate a multivariate distribution (for example, mass, surface area, amount of agglomeration) of a population of nanoparticles created in this process would help efforts to improve the final product and save energy.

Although it has been used in industry for decades,[4] the process is poorly understood and experimental optimization is incremental and costly. It has been demonstrated that the relative rates of gas-phase reactions, leading to particle nucleation, surface growth reactions, and particle agglomeration and sintering, are all important in determining the final product properties.[5] It is important that a comprehensive model includes details spanning all relevant length and time scales.

Existing models greatly simplify the chemical processes to a single step and are unable to capture the details of temperature and concentration dependencies. For example, the use of additives such as AlCl₃ and KCl to control the crystal structure and primary particle size of the product is common in industry,[6] but current modeling methods can offer no insight into the underlying processes.

As well as detailed chemistry on the molecular scale, it is clear that a detailed population balance model of the particles is desirable. Existing models range from simple monodisperse assumptions to two-dimensional (surface−volume) approaches simulating simultaneous nucleation, growth, agglomeration, and sintering. The ability to track primary and agglomerate sizes explicitly will allow the assumptions, such as monodisperse size distributions, that are currently used to model hard- and soft-agglomerate formation[7] to be relaxed.

The intention of this work is to create and demonstrate a framework for a comprehensive model that attempts to describe the phenomena at different scales. We present new results in three areas:

(1) Ab initio and density functional theory (DFT) investigations of the gas-phase chemistry of the combustion of TiCl₄ lay the foundation for the first detailed kinetic model of seed formation.

(2) A DFT study of the surface chemistry of rutile TiO₂ is undertaken as a first attempt to understand the surface growth of TiO₂ nanoparticles.

(3) A new population balance model extends existing surface-volume models to track primary particles within each agglomerate in the population. This detailed population balance model is coupled to the detailed chemistry with operator splitting and is solved using a stochastic technique.

The paper is structured as follows. After this introduction, the background to each of these three areas is described. In the following section, the models developed for the gas-phase chemistry and the detailed population balance are described. The subsequent results and discussion are again divided into the three areas: gas-phase chemistry, surface chemistry, and the detail population balance. These sections are followed by the conclusions.

* To whom correspondence should be addressed. Tel.: +44 (0)-1223 334777. Fax: +44 (0)1223 334796. E-mail address: mk306@cam.ac.uk.

2. Background

2.1. Gas-Phase Chemistry. Although the chloride process is a mature technology that has been used in industry since 1958, understanding of the gas-phase reactions of TiCl$_4$ oxidation remains incomplete.[8]

The overall stoichiometry of this process is

$$TiCl_4 + O_2 \rightarrow TiO_{2(nanoparticles)} + 2Cl_2 \qquad (1)$$

There have been a few experimental investigations of the kinetics of the system: Pratsinis et al.[9] reported the overall oxidation kinetics of TiCl$_4$ at 700−1000 °C. The rate was determined to be first-order with respect to TiCl$_4$, and was largely independent of O$_2$ concentration. This experimental work has been the basis for many theoretical studies of TiO$_2$ nanoparticle dynamics.[5,10−12] However, these experiments were performed at temperatures much lower than those used in the industrial process. Extrapolation of kinetic data to this degree must be treated with caution.

The only oxychloride intermediate to have been observed directly is TiOCl$_2$,[8,13] which suggests that it is likely to have an important role in the chemical mechanism.

Several chemical mechanisms have been proposed;[8,9] however, because of a lack of thermochemical data, no detailed simulations have previously been performed. Apart from the chlorides (TiCl$_y$), the only intermediate species with any published thermochemical data are TiOCl and TiOCl$_2$; these were estimated in 1963 with no explanation.[14] Our recent DFT quantum calculations have elucidated the necessary thermochemical data.[15] With estimates of the rate expressions for elementary reactions, this enables development of a kinetic mechanism for the gas-phase chemical reactions for the first time.

2.2. Surface Chemistry. TiO$_2$ is one of the most investigated metal oxide surfaces; details can be found in a recent comprehensive review article by Diebold.[16] Nevertheless, experimental investigations of the kinetics of the surface growth of rutile TiO$_2$ are scarce.

The rate of heterogeneous TiO$_2$ surface growth was investigated at temperatures of 400−850 °C,[17] and this first-order rate expression has been used in most modeling papers since.[5,10−12] However, this extrapolation to higher temperatures should be treated with caution, especially because a change in behavior at >850 °C is reported.[17] A more detailed understanding of the elementary steps involved in the surface growth will help to develop a more reliable universal rate expression.

It is generally believed that, after the seed is formed, TiCl$_4$ adsorbs and decomposes on the TiO$_2$ surface and, subsequently, molecular chlorine (Cl$_2$) desorbs, leaving Ti atoms on the surface.[5] This titanium-covered surface is then oxidized by molecular oxygen (O$_2$) and more TiCl$_4$ can adsorb and decompose. Bowker and co-workers investigated the kinetics of the reoxidation of reduced TiO$_2$\{110\};[18] however, the full cycle of the growth is not yet fully understood. A scheme of the presumed surface growth from layer n to layer $n + 1$ is given in Figure 1.

DFT has proven to be a useful tool for the elucidation of reactions and diffusion processes on metals[19−22] and metal oxides.[23−26] The details of the elementary-step reaction mechanism for the TiCl$_4$ decomposition and chlorine formation are not fully understood. This motivated an investigation of the surface chemistry using plane-wave DFT. The diffusion and desorption of chlorine from a TiO$_2$\{110\} surface (the region bordered by a dotted box in Figure 1) was recently studied.[27]
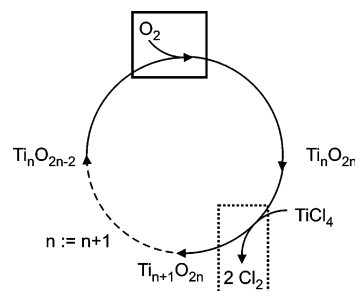

Figure 1. Surface reaction mechanism. The dotted box represents a section studied recently;[27] the solid box shows the section studied in this work.
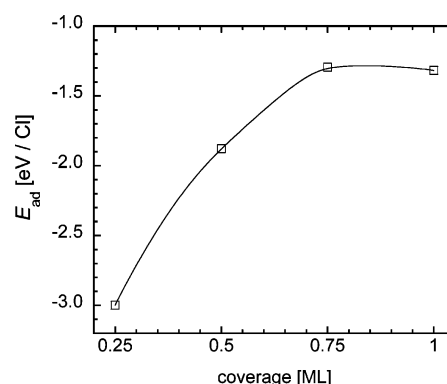

Figure 2. Chlorine adsorption on a reduced TiO$_2$\{110\} surface (from Inderwildi and Kraft[27]).

Figure 2, from Inderwildi and Kraft,[27] shows that the adsorption of chlorine on a reduced TiO$_2$\{110\} surface is strongly exothermic at all fractions of surface coverage: the desorption of chlorine from the reduced surface is energetically unfavorable at low temperatures. At high temperatures, such as those in the flame synthesis of TiO$_2$, however, the chlorine will desorb (Le Chatelier).

The work presented here extends this investigation to include the adsorption of oxygen on the reduced TiO$_2$\{110\} surface (the region bordered by a solid box in Figure 1).

2.3. Population Balances. Considering the surface area and size of the particles to be independent variables, nonspherical particle growth can be simulated using two-dimensional aerosol dynamics.[28] However, the nonlinear integro-differential equation, which describes the evolution of the two-dimensional particle size distribution (PSD), is difficult to solve directly; a summary of solution techniques is given in a review article by Kraft.[29]

Simultaneous surface growth, coagulation, and sintering in this TiO$_2$ synthesis process have previously been modeled using both sectional[28] and moving sectional[10] two-dimensional population balance models. Stochastic techniques have also been used to study this process,[12] as well as to study the population balance of soot formation in carbon systems, such as premixed laminar flames.[30] Stochastic techniques do not suffer from the numerical diffusion inherent in sectional methods, and, unlike moment methods, are able to provide the full multivariate particle population density without additional model constraints.

Such a stochastic population balance solver has been successfully coupled to a deterministic solver for the gas-phase chemistry using operator splitting.[31] This coupling allows stochastic simulations to compete in an area that, previously, was only accessible using sectional or moment methods.

The disadvantage of stochastic techniques for one-dimensional population balances is the additional computational time required for solution, although various algorithmic enhancements have been developed.[32] The major advantage of this stochastic

technique is the ease with which additional particle properties can be tracked, with a negligible increase in computational expense. This is used in the current work to develop an algorithm that enables the tracking of primary particles within each agglomerate particle, as will be described in section 3.2.

Stochastic algorithms offer the additional advantage of readily fitting into the standard computational fluid dynamics (CFD) framework, enabling the population balance to be elegantly coupled to the gas phase itself.[33] Typically, the Particle-In-Cell (PIC) method is adopted, which treats the particles as a local source of momentum, kinetic energy, and dissipation rate of turbulence. Although not all issues are resolved, it is hoped that, in this way, stochastic methods will be able to bridge the gap between phases and permit a complete description of the physics of TiO$_2$ production across the hierarchy of length scales to be obtained.

3. Model

This section describes the new developments in two separate aspects of the current work toward a comprehensive model.

3.1. Gas-Phase Chemistry. A detailed kinetic model consists of a list of intermediate species and the possible reactions between them. Each species must have thermochemical information, usually expressed in the form of polynomials for C_p, H, and S, and each reaction must have a forward rate expression, which is usually expressed in modified Arrhenius form, with the backward rate being calculated from the thermodynamic equilibrium constant.

The necessary thermochemical data for TiOCl, TiOCl$_2$, TiOCl$_3$, TiO$_2$Cl$_2$, TiO$_2$Cl$_3$, Ti$_2$O$_3$Cl$_3$, Ti$_2$O$_3$Cl$_2$, Ti$_2$O$_2$Cl$_3$, Ti$_3$O$_4$Cl$_4$, and Ti$_2$O$_2$Cl$_4$ were taken from recent quantum calculations;[15] those for TiCl$_3$, TiCl$_2$, and TiCl were taken from Hildenbrand;[34] and those for all other species were obtained from the National Aeronautics and Space Administration (NASA) database.[35,36]

Thermodynamic equilibrium calculations can give clues to the chemical mechanism. The most stable intermediate with only one Ti atom is TiOCl$_2$, which has an equilibrium mole fraction that is orders of magnitude higher than any other monomer species, other than the titanium chlorides. The most stable dimer species is Ti$_2$O$_2$Cl$_4$. Gaseous TiO$_2$ is unstable and will exist in very low concentrations. Therefore, the dimerization of TiOCl$_2$ to form Ti$_2$O$_2$Cl$_4$ is a more likely route to the formation of TiO$_2$ nanoparticles than the dimerization of gaseous TiO$_2$ molecules. The equilibrium calculations were used in this way to identify likely intermediate species and elementary steps in the reaction mechanism.

The elementary reactions of the species that contain one Ti atom can be grouped into several categories. (i) thermal decomposition, which initiates the radical reaction chain; (ii) radical abstraction of Cl and disproportionation; (iii) oxidation; and (iv) dimerization forming a Ti$_2$O$_x$Cl$_y$ species.

Starting with a list of species, all the feasible reactions were devised manually using the aforementioned categories as prompts, eliminating reactions that violate spin conservation. If any of the reactions generate new species, these were added to the list, their thermochemistry was calculated, and new reactions that they could perform were devised.

Table 1 shows the reactions considered in the mechanism, along with the standard enthalpy of reaction at 298 K and parameters for a modified Arrhenius rate expression for the forward rate coefficient,

$$k_f = A\left(\frac{T}{1\text{ K}}\right)^n \exp\left(\frac{E_a}{RT}\right) \qquad (2)$$

where T is the temperature (given in Kelvin).

The rate parameters for the initiating reactions (reactions R1 and R2 in Table 1) were taken from high-temperature shock tube experiments by Herzler and Roth,[37] which agree with values from a theoretical study by Teyssandier and Allendorf.[38] This study was also the source of the parameters for reaction R3.[38] Oxygen–chlorine chemistry in reactions R37–R44 was taken from the literature.[39–42]

The remaining rate parameters were estimated to have a pre-exponential factor, A, given by the collision limit 1×10^{13} mol cm^{-3} s^{-1}, and the activation energy (E_a) in the exothermic direction was taken to be zero. For this reason, all the reactions with estimated parameters are listed in the exothermic direction in Table 1.

This barrierless estimate provides an approximate upper limit for the reaction rates. For the radical combination reactions, this is a reasonable estimate. Work is underway to calculate the transition states of key reactions using quantum calculations, to determine more-accurate rate parameters. Some reactions that proceed via activated intermediates will probably be significantly slowed by falloff, and some chemically activated product channels will open. The effect of this will be estimated in future work; however, it is expected to affect reactions in which two species combine to form one species in the exothermic direction (reactions R19, R22, R23, R24, R45, and R50).

Our current mechanism includes 51 elementary reactions and oxidizes TiCl$_4$ to form a stable Ti$_2$O$_x$Cl$_y$ "dimer" species, which we believe lies on the path to TiO$_2$ nanoparticles. We shall continue this work to improve our rate estimates and extend the mechanism toward the stage where it can be directly coupled to the particle model with greater confidence.

3.2. Population Balance Modeling. To simulate the comprehensive model of chemistry and particle dynamics, the previous surface volume model[43] was extended to account for particle structure and coupled to the gas-phase chemistry simulation using operator splitting.[31] The gas-phase chemistry is solved deterministically using a standard ordinary differential equation (ODE) solver. The remainder of this section will describe the population balance model used to describe the particle population.

3.2.1. Particle Description. The current work extends a previous two-dimensional surface–volume model,[43] which provided some shape information about the particles and allowed particle sintering to be modeled. Using the surface–volume model for this system, a stochastic particle would be defined in the solver as a vector of TiO$_2$ monomer count and surface area; all other particle properties—and, hence, particle process rates—would be calculated from these. In this extension to the model, the sizes of the primary particles within each agglomerate particle are also tracked. Therefore, an agglomerate particle in the current population balance is described by the number of TiO$_2$ monomers in the particle (M), the surface area of the particle (A), and the number of TiO$_2$ monomers in each of the primary particles that make up the agglomerate (**m**) (**m** = m_1, m_2, m_3, ...). For each primary particle, the volume is found by multiplying the monomer count by the molar volume of rutile, and the surface area is determined by assuming that the primary particles are spherical.

For a simulation in which the highest number of primaries in a single agglomerate reaches N, the population balance effectively has ($N + 2 - 1$) dimensions (the -1 term is present

Table 1. Reaction Mechanism Equations

reaction number	reaction	ΔH°_{298K} (kJ/mol)	A (cm^3 mol^{-1} s^{-1})	n	E_a (kJ/mol)	reference
		Thermal Decomposition				
R1	$TiCl_4 + M \rightleftharpoons TiCl_3 + Cl + M$	387	5.40×10^{18}	0	336	Herzler and Roth[37]
R2	$TiCl_3 + M \rightleftharpoons TiCl_2 + Cl + M$	422	7.70×10^{18}	0	387	Herzler and Roth[37]
R3	$TiCl_2 + M \rightleftharpoons TiCl + Cl + M$	507	3.20×10^{17}	0	511	Teyssandier and Allendorf[38]
R4	$Ti + Cl \rightleftharpoons TiCl$	405	1.00×10^{13}	0	0	
R5	$TiCl_2 + Cl_2 \rightleftharpoons TiCl_4$	−567	1.00×10^{13}	0	0	
R6	$TiCl + Cl_2 \rightleftharpoons TiCl_3$	−687	1.00×10^{13}	0	0	
		Abstraction and Disproportionation				
R7	$TiCl_3 + Cl_2 \rightleftharpoons TiCl_4 + Cl$	−144	1.00×10^{13}	0	0	
R8	$TiCl_2 + Cl_2 \rightleftharpoons TiCl_3 + Cl$	−180	1.00×10^{13}	0	0	
R9	$TiCl + Cl_2 \rightleftharpoons TiCl_2 + Cl$	−265	1.00×10^{13}	0	0	
R10	$Ti + Cl_2 \rightleftharpoons TiCl + Cl$	−162	1.00×10^{13}	0	0	
R11	$TiCl_4 + TiCl \rightleftharpoons TiCl_3 + TiCl_2$	−121	1.00×10^{13}	0	0	
R12	$TiCl_4 + Ti \rightleftharpoons TiCl_3 + TiCl$	−18	1.00×10^{13}	0	0	
R13	$TiCl_2 + TiCl \rightleftharpoons TiCl_3 + Ti$	−17	1.00×10^{13}	0	0	
R14	$2TiCl \rightleftharpoons TiCl_2 + Ti$	−103	1.00×10^{13}	0	0	
R15	$Cl_2 + TiO_2 Cl_2 \rightleftharpoons Cl + TiO_2Cl_3$	−95	1.00×10^{13}	0	0	
R16	$Cl_2 + Ti_2 O_2Cl_3 \rightleftharpoons Cl + Ti_2O_2Cl_4$	−174	1.00×10^{13}	0	0	
R17	$2TiCl_3 \rightleftharpoons TiCl_2 + TiCl_4$	35	9.60×10^{12}	0	35	Herzler and Roth[37a]
R18	$TiCl_3 + TiCl \rightleftharpoons 2TiCl_2$	−85	1.00×10^{13}	0	0	
		Oxidation				
R19	$TiCl_3 + O_2 \rightleftharpoons TiO_2Cl_3$	−277	1.00×10^{13}	0	0	
R20	$TiOCl_3 + ClO \rightleftharpoons TiO_2 Cl_3 + Cl$	−115	1.00×10^{13}	0	0	
R21	$TiO_2Cl_3 + TiCl_3 \rightleftharpoons 2TiOCl_3$	−7	1.00×10^{13}	0	0	
R22	$TiOCl_2 + Cl \rightleftharpoons TiOCl_3$	−162	1.00×10^{13}	0	0	
R23	$TiOCl_3 + O \rightleftharpoons TiO_2Cl_3$	−384	1.00×10^{13}	0	0	
R24	$TiO_2Cl_2 + Cl \rightleftharpoons TiO_2 Cl_3$	−337	1.00×10^{13}	0	0	
R25	$TiO_2Cl_2 + Cl \rightleftharpoons TiCl_3 + O_2$	−61	1.00×10^{13}	0	0	
R26	$TiOCl_3 + O \rightleftharpoons TiCl_3 + O_2$	−108	1.00×10^{13}	0	0	
R27	$TiCl_2 + O_2 \rightleftharpoons TiOCl_2 + O$	−152	1.00×10^{13}	0	0	
R28	$TiO_2Cl_2 + O \rightleftharpoons TiOCl_2 + O_2$	−289	1.00×10^{13}	0	0	
R29	$TiCl_3 + ClO \rightleftharpoons TiCl_4 + O$	−118	1.00×10^{13}	0	0	
R30	$TiCl_2 + ClO \rightleftharpoons TiCl_3 + O$	−153	1.00×10^{13}	0	0	
R31	$TiCl + ClO \rightleftharpoons TiCl_2 + O$	−239	1.00×10^{13}	0	0	
R32	$Ti + ClO \rightleftharpoons TiCl + O$	−136	1.00×10^{13}	0	0	
R33	$TiCl_3 + O \rightleftharpoons TiOCl_2 + Cl$	−228	1.00×10^{13}	0	0	
R34	$TiCl_3 + Cl_2 O \rightleftharpoons TiCl_4 + ClO$	−243	1.00×10^{13}	0	0	
R35	$TiCl_3 + ClO \rightleftharpoons TiOCl_3 + Cl$	−122	1.00×10^{13}	0	0	
R36	$TiO_2 Cl_2 + Cl \rightleftharpoons TiOCl_2 + ClO$	−60	1.00×10^{13}	0	0	
		Cl/O Chemistry				
R37	$O + O_2 + M \rightleftharpoons O_3 + M$	−107	1.84×10^{21}	−2.8	0	Atkinson et al.[39]
R38	$ClOO + M \rightarrow Cl + O_2 + M$	24	1.69×10^{14}	0	15.13	Atkinson et al.[39]
R39	$Cl + O_2 + M \rightarrow ClOO + M$	−24	8.68×10^{21}	−2.9	0	Atkinson et al.[39]
R40	$Cl + O_3 \rightleftharpoons ClO + O_2$	−161	1.75×10^{13}	0	2.18	Atkinson et al.[40]
R41	$Cl_2 O + Cl \rightleftharpoons Cl_2 + ClO$	−99	3.73×10^{13}	0	−1.09	Atkinson et al.[40]
R42	$Cl + O_2 \rightleftharpoons ClO + O$	229	8.79×10^{14}	0	230.5	Baulch et al.[41]
R43	$O + Cl_2 \rightleftharpoons ClO + Cl$	−26	4.46×10^{12}	0	13.73	Wine et al.[42]
R44	$2Cl + M \rightleftharpoons Cl_2 + M$	−243	2.23×10^{14}	0	−7.53	Baulch et al.[41]
		Dimerization and Dimer Reactions				
R45	$2TiOCl_2 \rightleftharpoons Ti_2O_2Cl_4$	−356	1.00×10^{13}	0	0	
R46	$TiO_2Cl_2 + TiCl_3 \rightleftharpoons Ti_2O_2Cl_4 + Cl$	−375	1.00×10^{13}	0	0	
R47	$TiO_2Cl_2 + TiOCl_2 \rightleftharpoons Ti_2O_3Cl_3 + Cl$	−141	1.00×10^{13}	0	0	
R48	$TiOCl_2 + TiOCl_3 \rightleftharpoons Ti_2O_2Cl_4 + Cl$	−194	1.00×10^{13}	0	0	
R49	$Ti_2O_3Cl_3 + TiOCl_2 \rightleftharpoons Ti_3O_4Cl_4 + Cl$	−164	1.00×10^{13}	0	0	
R50	$Ti_2O_3Cl_2 + Cl \rightleftharpoons Ti_2O_3 Cl_3$	−208	1.00×10^{13}	0	0	
R51	$Ti_2O_2Cl_3 + TiCl_4 \rightleftharpoons Ti_2O_2Cl_4 + TiCl_3$	−29	1.00×10^{13}	0	0	

^{a}Estimate.

because $\sum_{i=1}^{N} m_i = M$). This expansion of the population balance to $N + 1$ dimensions ($N \approx 10^2$) rules out the use of sectional methods, in which the computation times scale exponentially with the number of dimensions. (A two-dimensional sectional simulation by Muhlenweg et al. for a similar system required ~112 days on a 300 MHz alpha workstation.[44]) The stochastic particle method used to solve the population balance makes it computationally inexpensive to track many internal coordinates within the population. The Linear Process Deferment Algorithm (LPDA) used here is explained by Patterson et al.[32] Similar to a direct simulation Monte Carlo (MC) algorithm, it requires only a set of rules for

creating and modifying the particles and their associated rates. We define these in sections 3.2.2−3.2.5.

3.2.2. Inception. At some point in the simulated growth mechanism, the collision and merging of two molecules to form a third will necessarily be treated as a particle coagulation event, rather than a gas-phase chemical reaction. Because the particle model does not include a breakage term, this coagulation is treated as being irreversible, unlike a gas-phase chemical reaction.

In the current study, the collision of any two molecules that contain two or more Ti atoms each is treated as a particle inception. The rate of these events is dependent on the

concentration of the species involved and is estimated according to collision theory, with the collision diameter estimated from the DFT results to be 0.65 nm (the diameter of the sphere with a volume equivalent to that occupied by the Connolly surface of $Ti_2O_2Cl_4$).

Studies of thermodynamic equilibrium composition based on the calculated thermochemistry[15] suggest that, at temperatures of >600 K, the critical nucleus size, above which molecules (or particles) prefer to grow than to shrink, probably contains at least five Ti atoms. In the present model, the transition from reversible gas-phase reaction to irreversible particle coagulation is premature, so the nucleation rate computed using this model is expected to be an overestimate. However, the present approach is a significant improvement over previous studies of this system which have treated the unstable triatomic molecule TiO_2 as a nucleated particle.[5,10−12]

When a particle is first incepted from the gas phase, it is assumed to be spherical, and its primary particle list is initiated with one entry whose size (monomer count) equals that of the incepted particle.

For example, the inception reaction

$$Ti_2O_2Cl_4 + Ti_2O_3Cl_2 \rightarrow \underbrace{(TiO_2)_4}_{\text{particle}} + 3Cl_2 - 1.5O_2 \quad (3)$$
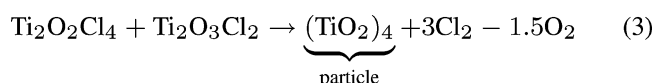
would create a particle with the properties

$$M = \text{number of Ti atoms} = 4 \quad (4)$$

$$A = \pi^{1/3}\left(\frac{6M}{\rho}\right)^{2/3} \quad (5)$$

$$m_1 = M \quad (6)$$

where ρ is the molar density of bulk rutile.

3.2.3. Surface Growth. Although progress is being made toward a better understanding of the surface chemistry of this system, because of a lack of kinetic data, the current population balance uses the commonly used[5,10−12] one-step expression given by Ghoshtagore:[17]

$$\frac{dM}{dt} = A \times [TiCl_4] \times (4.9 \times 10^3 \text{ cm s}^{-1}) \times$$
$$\exp\left(\frac{-74.8 \text{ kJ/mol}}{k_B T}\right) \quad (7)$$

where A is the surface area of the particle, $[TiCl_4]$ the concentration of $TiCl_4$ in the gas phase, T the temperature, and k_B the Boltzmann constant.

When chemical reactions on the surface increase the number of TiO_2 monomer units in a particle by a number ΔM, the volume of the particle increases by $\Delta M/\rho$, where ρ is the molar density of bulk rutile. For nonspherical particles, the effect this surface growth has on the surface area of the particle (dA/dM and, thus, dA/dt) is less obvious. To calculate this value, we use the radius-of-curvature method explained by Patterson and Kraft.[43] This model causes surface reactions to increase the sphericity of particles, as suggested by transmission electron microscopy (TEM) images of soot particles.

When surface growth is determined to have added a certain number (ΔM) of monomer units to a particle, these are distributed among the constituent primary particles randomly, with probabilities proportional to their spherical surface areas ($p_i \propto m_i^{2/3}$).
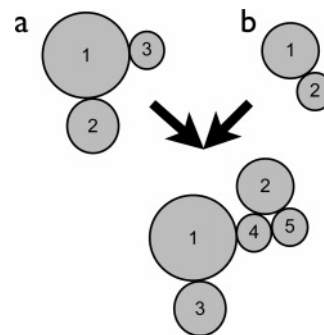

Figure 3. Coagulation of particles a and b.

3.2.4. Coagulation. The rates of collisions between particles of different sizes and shapes is determined by the coagulation kernel, which, in this case, is a function of M and A. Different coagulation kernels are appropriate under different conditions (particle size and gas pressure). (See the work of Singh et al.[45] for details.) These coagulation kernels are also used to model the particle inception processes.

When two particles coagulate, the monomer count and surface area are conserved, and the lists of constituent primary particles are appended to each other. For example, when two particles a and b, with properties (M_a, A_a, m_{a1}, m_{a2}, m_{a3}) and (M_b, A_b, m_{b1}, m_{b2}), coagulate as illustrated in Figure 3, the resulting agglomerate particle will be given by

$$M = M_a + M_b$$

$$A = A_a + A_b$$

$$m_1 = m_{a1}$$

$$m_2 = m_{b1}$$

$$m_3 = m_{a2}$$

$$m_4 = m_{a3}$$

$$m_5 = m_{b2}$$

3.2.5. Sintering. To model sintering, we follow the approach of Xiong and Pratsinis[28] and assume that the excess agglomerate surface area, over that of a spherical particle with the same mass, decays exponentially:

$$\frac{dA}{dt} = -\frac{1}{\tau_f}\left[A - \pi^{1/3}\left(\frac{6M}{\rho}\right)^{2/3}\right] \quad (8)$$

As in previous works,[12,28] the characteristic time was given by the expression for TiO_2 particles sintering through grain-boundary diffusion that was obtained by Kobata et al.:[46]

$$\tau_f = 7.4 \times 10^8 \text{ K}^{-1} T d_p^4 \exp\left(\frac{3.1 \times 10^4 \text{ K}}{T}\right) \quad (9)$$

where d_p is a measure of the average primary particle diameter ($d_p = 6M/\rho A$).

As specified previously, the surface area of an aggregate particle in this simulation is tracked independently and determined by the sintering and surface growth models. The list of primary particles is updated to match this surface area value according to the following scheme, inspired by Ostwald ripening (see Figure 4):
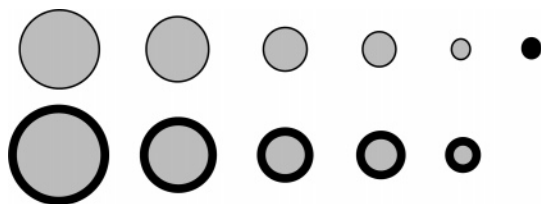
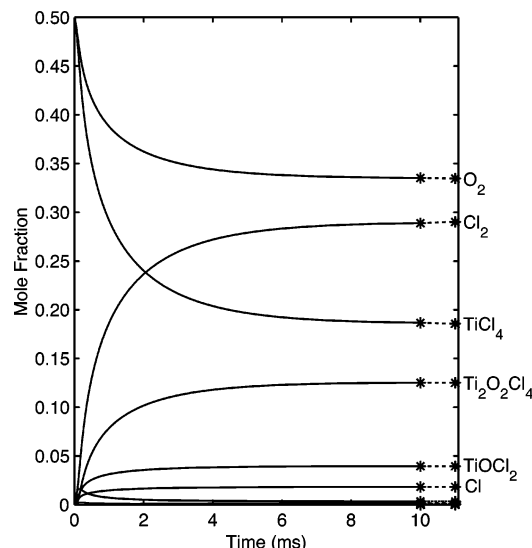**Figure 4.** Primary particles before (top) and after (bottom) sintering.

Figure 5. Species mole fractions versus time. Initial composition was 50 mol % TiCl$_4$ in O$_2$ at time $t = 0$ and constant temperature and pressure ($T = 1500$ K, $P = 3 \times 10^5$ Pa) The dashed line to the final data point shows the mole fraction at thermodynamic equilibrium.

Table 2. Kinetic Sensitivity Analysis

reaction number	reaction	sensitivity[a]
R21	TiO$_2$Cl$_3$ + TiCl$_3$ ⇌ 2TiOCl$_3$	0.24
R1	TiCl$_4$ + M ⇌ TiCl$_3$ + Cl + M	0.05
R35	TiCl$_3$ + ClO ⇌ TiOCl$_3$ + Cl	0.05
R7	TiCl$_3$ + Cl$_2$ ⇌ TiCl$_4$ + Cl	0.05
R19	TiCl$_3$ + O$_2$ ⇌ TiO$_2$Cl$_3$	0.007
R47	TiO$_2$Cl$_2$ + TiOCl$_2$ ⇌ Ti$_2$O$_3$Cl$_3$ + Cl	−0.007
R20	TiOCl$_3$ + ClO ⇌ TiO$_2$Cl$_3$ + Cl	0.005

[a] Sensitivity = $\Delta(\log(x_{1\,ms}))/\Delta(\log(A))$, where $x_{1\,ms}$ is the mole fraction of Ti$_2$O$_2$Cl$_4$ at $t = 1$ ms and A is the pre-exponential factor for the reaction rate (see eq 2).

(1) If the sum of the primary particle surface areas exceeds the required aggregate surface area, then go to step 2; otherwise, end.

(2) Select the smallest primary particle.

(3) Remove this primary particle from the list, noting its monomer count (size).

(4) Redistribute the monomers across the other primary particles randomly, with probabilities in proportion to their surface areas.

(5) Recalculate the surface areas of the primary particles.

(6) Go to step 1.

3.2.6. Shape Estimation. To generate shape information, for the purpose of aiding visualization of the particles, the positions of the primary particles within a particle are generated in a post-processing step. The primary particles are shuffled in a random order and one of them is placed at the origin. The remaining primary particles are placed according to this algorithm:

(1) The center of mass is found for the primary particles that have already been placed.

(2) A vector from this center of mass is chosen in a random direction.

(3) The next primary particle is placed on this vector in a position where it just touches an already placed primary particle.

4. Results and Discussion

4.1. Gas-Phase Chemistry. The chemical mechanism, thermochemistry, and rate parameters previously described were used to simulate a zero-dimensional batch reactor at constant temperature and pressure (1500 K, 3×10^5 Pa) with an initial mixture of 50 mol % TiCl$_4$ in O$_2$. These conditions are similar to those observed in a typical industrial reactor.[6,47] The simulation was performed using Cantera.[48] The time evolutions of the species mole fractions over the first 10 ms are shown in Figures 5 and 6. The overall process is the conversion of TiCl$_4$ into the dimer species Ti$_2$O$_2$Cl$_4$ (Figure 5). Figure 6 is plotted on a logarithmic scale and shows the details of the reactive intermediates.

The main reaction sequence (Figure 7) begins with the formation of TiCl$_3$ radicals from TiCl$_4$, primarily via radical abstraction (the reverse of reaction R7 in Table 1, hereinafter denoted as R7′),
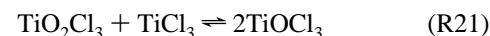
$$\text{TiCl}_4 + \text{Cl} \rightleftharpoons \text{TiCl}_3 + \text{Cl}_2 \quad (\text{R7}')$$
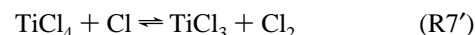
but also via pressure-dependent thermal decomposition (R1 in the forward direction):

$$\text{TiCl}_4 + \text{M} \rightleftharpoons \text{TiCl}_3 + \text{Cl} + \text{M} \quad (\text{R1})$$
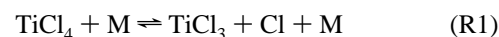
These TiCl$_3$ radicals are then oxidized to give TiOCl$_3$, some directly,

$$\text{TiCl}_3 + \text{ClO} \rightleftharpoons \text{TiOCl}_3 + \text{Cl} \quad (\text{R35})$$

but the majority via TiO$_2$Cl$_3$:

$$\text{TiCl}_3 + \text{O}_2 \rightleftharpoons \text{TiO}_2\text{Cl}_3 \quad (\text{R19})$$

$$\text{TiO}_2\text{Cl}_3 + \text{Cl} \rightleftharpoons \text{TiOCl}_3 + \text{ClO} \quad (\text{R20}')$$

$$\text{TiO}_2\text{Cl}_3 + \text{TiCl}_3 \rightleftharpoons 2\text{TiOCl}_3 \quad (\text{R21})$$

TiOCl$_3$ reacts to form the more stable intermediate TiOCl$_2$ via

$$\text{TiOCl}_3 \rightleftharpoons \text{TiOCl}_2 + \text{Cl} \quad (\text{R22}')$$
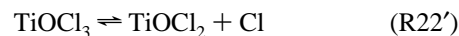
After a sufficient amount of TiOCl$_2$ has formed, it dimerizes to form Ti$_2$O$_2$Cl$_4$:

$$2\text{TiOCl}_2 \rightleftharpoons \text{Ti}_2\text{O}_2\text{Cl}_4 \quad (\text{R45})$$
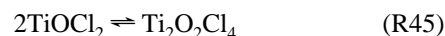
This is a first step toward a nanoparticle that contains thousands of TiO$_2$ units.

4.1.1. Sensitivity Analysis. The sensitivity of the overall reaction rate was investigated with respect to changes in both the individual rate coefficients of each reaction and the thermochemistry of each species. A 1:1 molar ratio of O$_2$ and TiCl$_4$ was simulated at 3×10^5 Pa and 1500 K, and the mole fraction of the dimer Ti$_2$O$_2$Cl$_4$ at $t = 1$ ms was noted.

Increasing the rate of reaction R21 (both forward and reverse, i.e., fixed thermochemistry) by a factor of 3 increases the mole fraction of the dimer after 1 ms by 30% (see Table 2). A few other rate constants also noticeably affect the dimer formation kinetics. However, generally, the kinetics is relatively insensitive to the assumed rate constants.
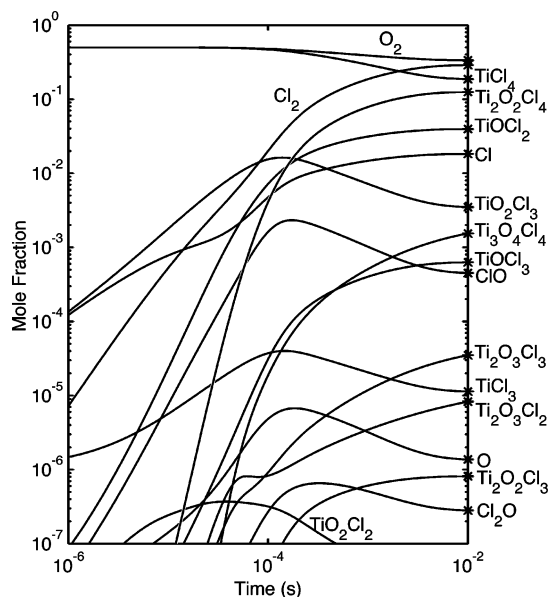
Figure 6. Species mole fractions (logarithmic) versus time (logarithmic). Starting composition was 50 mol % $TiCl_4$ in O_2 at time $t = 0$ and constant temperature and pressure ($T = 1500$ K, $P = 3 \times 10^5$ Pa).

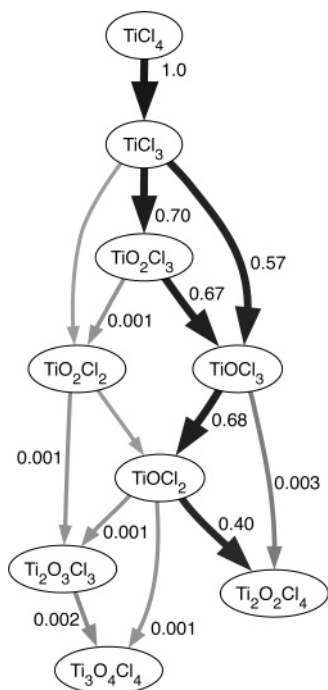**Figure 7.** Main reaction paths, showing the relative net flux of species at 72 μs, by which time 1% of the $Ti_2O_2Cl_4$ has been formed.

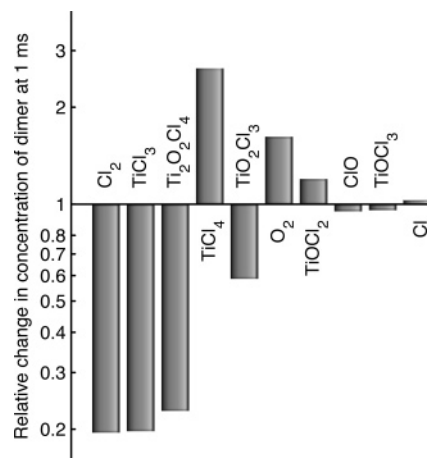**Figure 8.** Sensitivity of the concentration of $Ti_2O_2Cl_4$ after 1 ms to a 50 kJ/mol increase in the enthalpy of formation of each species, at constant temperature and pressure ($T = 1500$ K, $P = 3 \times 10^5$ Pa).
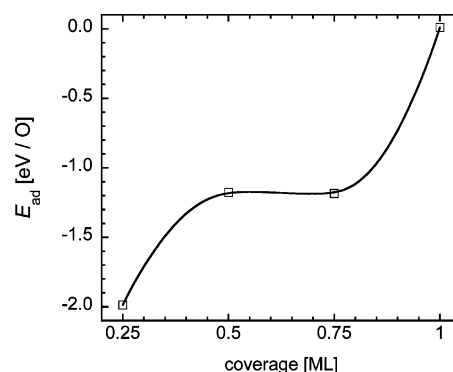

Figure 9. Oxygen adsorption on a reduced $TiO_2\{110\}$ surface.

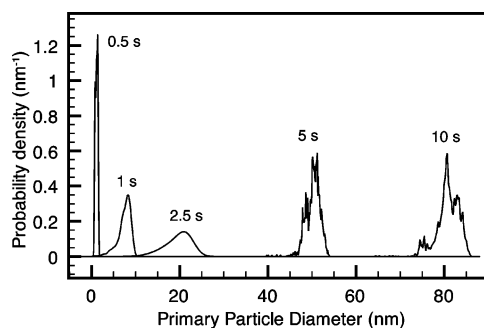**Figure 10.** Primary particle size distribution (mass-weighted) after various times at 800 °C.

The kinetics are naturally sensitive to the enthalpies of formation of $TiCl_4$, O_2, and Cl_2; however, fortunately, all of these are very well-established. Of the species with poorly established thermochemistry, the kinetics are most sensitive to the enthalpies of $TiCl_3$ and the dimer $Ti_2O_2Cl_4$; making either species 50 kJ less stable decreases the concentration of $Ti_2O_2Cl_4$ after 1 ms by a factor of ~5. The other titanium-containing species have a much weaker effect on the predicted kinetics (see Figure 8).

Hildenbrand[34] has persuasively argued that the NASA[49] and JANAF[14] enthalpies for $TiCl_3$ are inaccurate by ~42 kJ/mol at 298 K; using the JANAF estimate for $TiCl_3$, rather than Hildenbrand's estimate, increases the overall reaction rate by ~12%. Our DFT-based estimate of the enthalpy of formation of $Ti_2O_2Cl_4$ is unfortunately the only value in the literature;

because there is no reliable reference species available on which to base an isodesmic reaction, a value of 50 kJ/mol is a reasonable estimate of the uncertainty.

4.2. Surface Chemistry. In addition to the investigation of the seed formation in the gas phase using orbital-centered DFT, plane-wave DFT calculations were applied to study the growth process of rutile TiO_2 surfaces. Details of the calculation methods are given by Inderwildi and Kraft.[27] Two stages of the surface growth of TiO_2 have now been studied. First, the diffusion and desorption of chlorine (formed via the decomposition of $TiCl_4$) from a $TiO_2\{110\}$ surface was studied.[27] In this work, the adsorption of oxygen on reduced $TiO_2\{110\}$ was also studied.

Figure 9 shows the average adsorption energy of oxygen on a reduced $TiO_2\{110\}$ surface, as function of the surface coverage. Oxidation of the reduced $TiO_2\{110\}$ is initially energetically very favorable, and the formation of a stoichio-
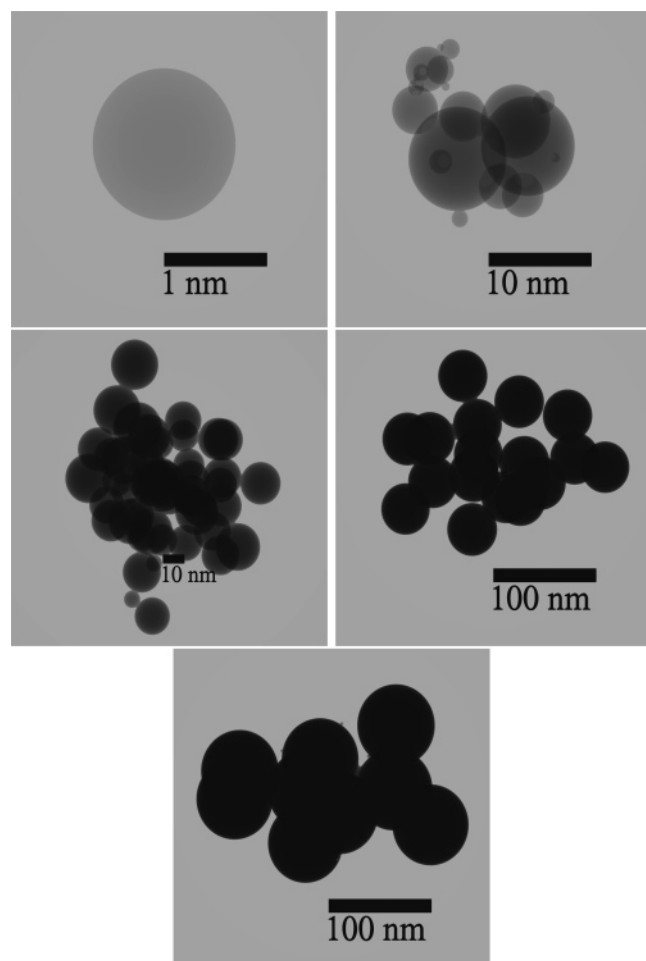
Figure 11. Transmission electron microscopy (TEM)-style images of the oldest particle in the simulation after 0.5, 1, 2.5, 5, and 10 s at 800 °C.
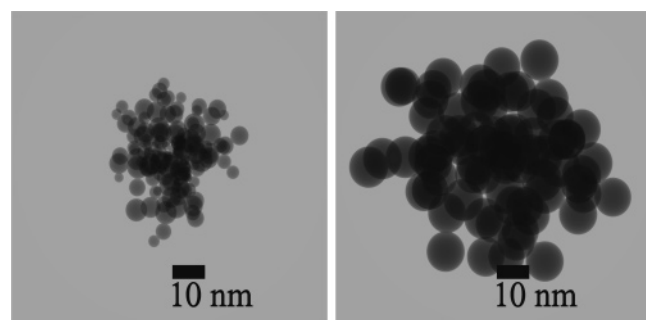

Figure 12. TEM-style images of the oldest particle after 0.1 and 0.2 ms in the industrial reactor simulation.

metric surface is still favorable (coverage = 0.5 ML), while the full oxidation is thermoneutral. This oxidation of reduced $TiO_2\{110\}$ will be a crucial step in the synthesis of rutile TiO_2, because the decomposition of $TiCl_4$ or the oxychloride species will be rather fast, while the results presented here indicate that the oxidation (especially the full oxidation) is presumably slow, compared to the $TiCl_4$ decomposition, because the full oxidation is overall thermoneutral (BEP relation).[50]

We believe this work will lead to an improved understanding of the surface growth mechanism that can be used directly in population balance modeling.

4.3. Coupled Gas-Phase and Particle Simulation. The combined simulation coupling the gas-phase kinetic model to the particle dynamics model was used to simulate the tubular-flow reactor described by Pratsinis.[9] Figure 10 shows the
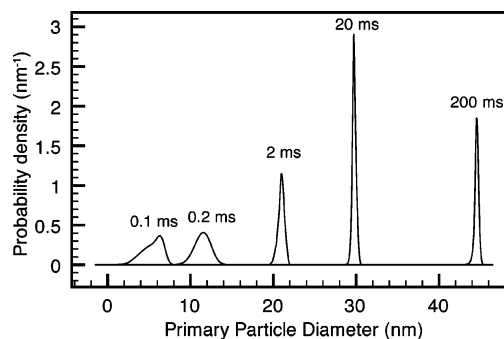

Figure 13. Primary particle size distributions (mass weighted) at various times in the industrial reactor simulation.

evolution of the primary particle size distribution from a simulation of a plug flow reactor at constant temperature of 800 °C, starting with a feed of 0.2 mol % $TiCl_4$ and 1 mol % O_2 in an argon carrier gas. The simulation used the developmental gas-phase mechanism from section 3.1, with surface chemistry from Ghoshtagore,[17] coupled to the population balance described in section 3.2. To give an indication of the possible shapes of the agglomerate particles, Figure 11 shows TEM-style images of the first particle from the same simulation. The geometric information was generated as described previously.

Because the kinetic model is thought to be incomplete and has not had any free parameters adjusted to fit experimental data, the time scales on the simulation are likely to be inaccurate. According to the simulation, after 0.5 s, most of the particles are newly incepted and so the primary particle size distribution is very narrow and the average diameter is very small: the particles are essentially all $(TiO_2)_4$ molecules. After 1 s, the particles have had opportunities to coagulate and form agglomerates. Those primary particles that coagulated early will have also had sufficient time to sinter together and to grow through surface reactions. However, there are still many new primary particles nucleating from the gas phase at this stage. The primary particle size distribution is seen to grow and broaden, both within the population (Figure 10) and within individual particles (Figure 11). Although the flow time through the experimental reactor was ∼ 1 s, the simulation was continued until 10 s. After 5 s, the average primary particle diameter has increased to ∼50 nm. The absolute width of the distribution is similar to that after 1 s, so the relative width is much narrower, which leads to a much more monodisperse appearance, as observed in the TEM-style images. This trend continues up to 10 s, by which time the primary particles have attained a diameter of ∼80 nm.

The simulation was repeated for conditions more similar to those of an industrial reactor: an equimolar ratio of $TiCl_4$ and O_2 fed to a plug-flow reactor at 3×10^5 Pa pressure, with a temperature profile constant at 1500 K for 100 ms, falling linearly to 1000 K over the next 100 ms.

The very high concentration of reactants and high temperature causes a large burst of particle inception, peaking at 0.1 ms. Particles from 0.1 and 0.2 ms are shown in Figure 12. Within 0.4 ms, 90% of the $TiCl_4$ is consumed and the inception rate has dropped to 0.5% of its peak value. This rapid burst of particle inception near the beginning of the reactor leads to a very narrow primary particle size distribution (Figure 13). After 200 ms, most primary particles in the simulation have a diameter of ∼45 nm.[47] Pigmentary titania from industrial reactors, after an additional 10 s in a plug-flow cooler, typically has an average primary particle size of 250 nm. Given the approximations in

the current set of sub-models, this level of agreement is encouraging.

5. Conclusions

Significant progress has been made from first principles toward a comprehensive model of the combustion of TiCl$_4$ to form TiO$_2$ particles, which is one of the largest volume processes using combustion synthesis.

Using recently published thermochemical data for the TiCl$_x$O$_y$ intermediates,[15] the present work demonstrates, for the first time, that it is possible to construct sensible, thermodynamically consistent kinetic models for this important process. As a start, an approximate kinetic model was constructed using the new thermochemistry; this model was determined to be at least qualitatively correct, rapidly converting TiCl$_4$ to oxygen-containing dimers. Additional work is required to detail the subsequent chemistry of the dimers and trimers. The model predictions fortunately are not sensitive to the assumed rate parameters, although the model certainly would be improved by the inclusion of falloff effects. The model predictions are fairly sensitive to the thermochemistry of the TiCl$_3$ and Ti$_2$O$_2$Cl$_4$ intermediates.

Plane-wave density functional theory (DFT) investigations of the oxygen and chlorine adsorption on rutile TiO$_2$\{110\} showed that the oxidation of the reduced TiO$_2$\{110\} surface might be the rate-determining step in the formation of bigger nanoparticles: first, because the barrier for the adsorption of oxygen is the highest, and, second, because the presented study indicates that oxygen "pushes" the chlorine into a position from which it can desorb more easily. These findings lead toward a better understanding of the surface mechanism, which will, in turn, lead to an improved kinetic model for surface reactions in this system.

A new multivariate population balance model was devised in which, in addition to surface area and volume, the size of every primary particle within each agglomerate particle in the population is tracked. The population balance model was solved using a stochastic particle algorithm coupled to the detailed gas-phase chemical mechanism using an operator splitting technique. This new population balance model allows the primary particle size distribution to be followed explicitly, and simple postprocessing generates spatial information, presented here in the form of transmission electron microscopy (TEM)-style images.

By coupling a new detailed kinetic model, generated from quantum chemical calculations, to a new population balance model with primary particle tracking, the current work demonstrates the feasibility of using first-principles modeling to tackle industrially important chemical engineering questions.

Recent advances in population balance modeling are such that further work on developing a kinetic model for the chemical mechanism could now have a real impact on the ability to predict important product properties, such as paint opacity; theoretical work toward such a kinetic model would be greatly assisted by new experimental data recorded under well-defined conditions.

Acknowledgment

Literature Cited

(1) Emsley, J. *Molecules at an Exhibition*; Oxford University Press: Oxford, U.K., 1999.

(2) Gonzalez, R. A.; Musick, C. D.; Tilton, J. N. Process for controlling agglomeration in the manufacture of TiO$_2$. U.S. Patent 5,508,015, April 16, 1996.

(3) Deberry, J. C.; Robinson, M.; Pomponi, M. D.; Beach, A. J.; Xiong, Y.; Akhtar, K. Controlled vapor phase oxidation of titanium tetrachloride to manufacture titanium dioxide. U.S. Patent 6,387,347, May 14, 2002.

(4) Willcox, O. B. Method and means for commingling and reacting fluid substances. U.S. Patent 2,791,490, May 7, 1957.

(5) Pratsinis, S. E.; Spicer, P. T. Competition between gas phase and surface oxidation of TiCl$_4$ during synthesis of TiO$_2$ particles—a two dimensional solution of the population balance equation. *Chem. Eng. Sci.* **1998**, *53*, 1861.

(6) Allen, A.; Evers, G. R. TiO$_2$ manufacturing process. U.S. Patent 5,201,949, April 13, 1993.

(7) Grass, R.; Tsantilis, S.; Pratsinis, S. Design of High-Temperature, Gas-Phase Synthesis of Hard or Soft TiO$_2$ Agglomerates. *AIChE J.* **2006**, *52*, 1318.

(8) Karlemo, B.; Koukkari, P.; Paloniemi, J. Formation of gaseous intermediates in titanium(IV) chloride plasma oxidation. *Plasma Chem. Plasma Process.* **1996**, *16*, 59.

(9) Pratsinis, S. E.; Bai, H.; Biswas, P.; Frenklach, M.; Mastrangelo, S. V. R. Kinetics of Titanium(IV) Chloride Oxidation. *J. Am. Ceram. Soc.* **1990**, *73*, 2158.

(10) Spicer, P. T.; Chaoul, O.; Tsantilis, S.; Pratsinis, S. E. Titania formation by TiCl$_4$ gas phase oxidation, surface growth and coagulation. *J. Aerosol Sci.* **2002**, *33*, 17.

(11) Tsantilis, S.; Pratsinis, S. E. Narrowing the size distribution of aerosol-made titania by surface growth and coagulation. *J. Aerosol. Sci.* **2004**, *35*, 405.

(12) Morgan, N.; Wells, C.; Goodson, M.; Kraft, M.; Wagner, W. A new numerical approach for the simulation of the growth of inorganic nanoparticles. *J. Comput. Phys.* **2006**, *211*, 638.

(13) Hildenbrand, D. L.; Lau, K. H.; Mastrangelo, S. V. R. Gaseous species in the Ti—Al—Cl system and reaction with H$_2$O. *J. Phys. Chem.* **1991**, *95*, 3435.

(14) Chase, M. W., Jr. NIST—JANAF Thermochemical Tables—Monograph 9. *J. Phys. Chem. Ref. Data* **1998**, *27*, 1951.

(15) West, R. H.; Beran, G. J. O.; Green, W. H.; Kraft, M. First-principles thermochemistry for the production of TiO$_2$ from TiCl$_4$. *J. Phys. Chem. A* **2007**, *111*, 3560.

(16) Diebold, U. The surface science of titanium dioxide. *Surf. Sci. Rep.* **2003**, *48*, 53.

(17) Ghoshtagore, R. N. Mechanism of heterogeneous deposition of thin film rutile. *J. Electrochem. Soc.* **1970**, *117*, 529.

(18) Smith, R. D.; Bennett, R. A.; Bowker, M. Measurement of the surface-growth kinetics of reduced TiO$_2$(110) during reoxidation using time-resolved scanning tunneling microscopy. *Phys. Rev. B: Condens. Matter Mater. Phys.* **2002**, *66*, 035409.

(19) Mavrikakis, M.; Rempel, J.; Greeley, J.; Hansen, L.; Nørskov, J. Atomic and molecular adsorption on Rh(111). *J. Chem. Phys.* **2002**, *117*, 6737.

(20) Liu, Z.-P.; Jenkins, S. J.; King, D. A. Car Exhaust Catalysis from First Principles: Selective NO Reduction under Excess O$_2$ Conditions on Ir. *J. Am. Chem. Soc.* **2004**, *126*, 10746.

(21) Inderwildi, O. R.; Lebiedz, D.; Deutschmann, O.; Warnatz, J. Coverage dependence of oxygen decomposition and surface diffusion on rhodium(111): A DFT study. *J. Chem. Phys.* **2005**, *122*, 034710.

(22) Inderwildi, O. R.; Lebiedz, D.; Deutschmann, O.; Warnatz, J. Influence of Coadsorbates on the NO Dissociation on a Rhodium(311) Surface. *ChemPhysChem* **2005**, *6*, 2513.

(23) Rasmussen, M.; Molina, L.; Hammer, B. Adsorption, diffusion, and dissociation of molecular oxygen at defected TiO$_2$(110): A density functional theory study. *J. Chem. Phys.* **2004**, *120*, 988.

(24) Tutuianu, M.; Inderwildi, O. R.; Bessler, W. G.; Warnatz, J. Competitive Adsorption of NO, NO$_2$, CO$_2$, and H$_2$O on BaO(100): A Quantum Chemical Study. *J. Phys. Chem. B* **2006**, *110*, 17484.

(25) Broqvist, P.; Panas, I.; Grönbeck, H. Toward a realistic description of NO$_x$ storage in BaO: The aspect of BaCO$_3$. *J. Phys. Chem. B* **2005**, *109*, 9613.

(26) Liu, Z.; Gong, X.; Kohanoff, J.; Sanchez, C.; Hu, P. Catalytic Role of Metal Oxides in Gold-Based Catalysts: A First Principles Study of CO Oxidation on TiO$_2$ Supported Au. *Phys. Rev. Lett.* **2003**, *91*, 266102.

(27) Inderwildi, O.; Kraft, M. Adsorption, Diffusion and Desorption of Chlorine on and from Rutile TiO$_2$\{110\}: A Theoretical Investigation. *ChemPhysChem* **2007**, *8*, 444.

(28) Xiong, Y.; Pratsinis, S. E. Formation of agglomerate particles by coagulation and sintering—Part I. A two-dimensional solution of the population balance equation. *J. Aerosol Sci.* **1993**, *24*, 283.

(29) Kraft, M. Modelling of Particulate Processes. *KONA* **2005**, *23*, 18.

(30) Balthasar, M.; Kraft, M. A stochastic approach to calculate the particle size distribution function of soot particles in laminar premixed flames. *Combust. Flame* **2003**, *133*, 289.

(31) Celnik, M.; Patterson, R.; Kraft, M.; Wagner, W. Coupling a stochastic soot population balance to gas-phase chemistry using operator splitting. *Combust. Flame* **2007**, *148*, 158.

(32) Patterson, R.; Singh, J.; Balthasar, M.; Kraft, M.; Norris, J. R. The Linear Process Deferment Algorithm: A new technique for solving population balance equations. *SIAM J. Sci. Comput.* **2006**, *28*, 303.

(33) Vikhansky, A.; Kraft, M. Modelling of a RDC using a combined CFD—population balance approach. *Chem. Eng. Sci.* **2003**, *59*, 2597.

(34) Hildenbrand, D. L. Thermochemical properties of gaseous TiCl, TiCl$_2$, and TiCl$_3$. *High Temp. Mater. Sci.* **1996**, *35*, 151.

(35) Gordon, S.; McBride, B. J. Computer Program for Calculation of Complex Chemical Equilibrium Composition, Rocket Performance, Incident and Reflected Shocks and Chapman—Jouguet Detonations. Technical Report NASA-TP-273, NASA—Glenn Research Center, Cleveland, OH, 1976.

(36) McBride, B. J.; Gordon, S.; Reno, M. A. Coefficients for Calculating Thermodynamic and Transport Properties of Individual Species. Technical Report NASA TM-4513, NASA—Glenn Research Center, Cleveland, OH, 1993.

(37) Herzler, J.; Roth, P. High-temperature decomposition of TiCl$_4$ based on Cl$^-$ concentration measurements. *Proc. Combust. Inst.* **2003**, *29*, 1353.

(38) Teyssandier, F.; Allendorf, M. D. Thermodynamics and kinetics of gas-phase reactions in the Ti—Cl—H system. *J. Electrochem. Soc.* **1998**, *145*, 2167.

(39) Atkinson, R.; Baulch, D. L.; Cox, R. A.; Hampson, R. F.; Kerr, J. A.; Rossi, M. J.; Troe, J. Evaluated kinetic and photochemical data for atmospheric chemistry: Supplement VI—IUPAC subcommittee on gas kinetic data evaluation for atmospheric chemistry. *J. Phys. Chem. Ref. Data* **1997**, *26*, 1329.

(40) Atkinson, R.; Baulch, D. L.; Cox, R. A.; Hampson, R. F.; Kerr, J. A.; Rossi, M. J.; Troe, J. Summary of Evaluated Kinetic and Photochemical Data for Atmospheric Chemistry, 2001. (URL: www.iupac-kinetic.ch.cam.ac.uk)

(41) Baulch, D. L.; Duxbury, J.; Grant, S. J.; Montague, D. C. Evaluated kinetic data for high temperature reactions. Volume 4. Homogeneous gas phase reactions of halogen- and cyanide-containing species. *J. Phys. Chem. Ref. Data* **1981**, *10*, 1.

(42) Wine, P. H.; Nicovich, J. M.; Ravishankara, A. R. Kinetics of the Reactions of O(^{3}P) and O(^{1}D) with Cl$_2$. *J. Phys. Chem.* **1985**, *89*, 3914.

(43) Patterson, R. I. A.; Kraft, M. Models for the aggregate structure of soot particles. *Combust. Flame* **2007**, in press. (DOI: 10.1016/j.combust-flame.2007.04.012)

(44) Mühlenweg, H.; Gutsch, A.; Schild, A.; Pratsinis, S. E. Process simulation of gas-to-particle-synthesis via population balances: Investigation of three models. *Chem. Eng. Sci.* **2002**, *57*, 2305.

(45) Singh, J.; Patterson, R. I. A.; Balthasar, M.; Kraft, M.; Wagner, W. Modelling soot particle size distribution: Dynamics of pressure regimes. Technical Report 25, c4e Cambridge Preprint Series, 2004.

(46) Kobata, A.; Kusakabe, K.; Morooka, S. Growth and transformation of TiO$_2$ crystallites in aerosol reactor. *AIChE J.* **1991**, *37*, 347.

(47) Edwards, J. Huntsman Pigments, Tioxide Europe, Ltd. Personal communication, 2007.

(48) Goodwin, D. G. An open source, extensible software suite for CVD process simulation. In *Vapor Disposition XVI and EUROCVD 14*; Allendorff, M., Maury, F., Teyssandier, F., Eds.; *ECS Proceedings, Vol. 2003—08*; The Electrochemical Society: Pennington, NJ, 2003; pp 155—162. (URL: www.cantera.org.)

(49) McBride, B. J.; Zehe, M. J.; Gordon, S. NASA Glenn Coefficients for Calculating Thermodynamic Properties of Individual Species. Technical Report NASA TP-2002—211556, NASA—Glenn Research Center, Cleveland, OH, 2002.

(50) Inderwildi, O.; Lebiedz, D.; Warnatz, J. Linear relationship between activation energies and reaction energies for coverage-dependent dissociation reactions on rhodium surfaces. *Phys. Chem. Chem. Phys.* **2005**, *7*, 2552.